Supplementary Information

for

Nanoribbons with Nonalternant Topology from Fusion of Polyazulene: Carbon Allotropes Beyond Graphene

Qitang Fan[1‡], Daniel Martin-Jimenez[2,3‡], Daniel Ebeling[2,3*], Claudio K. Krug[1], Lea Brechmann[1], Corinna Kohlmeyer[4], Gerhard Hilt[4*], Wolfgang Hieringer[5*], André Schirmeisen[2,3], J. Michael Gottfried[1*]

[1]Department of Chemistry, Philipps University Marburg, Hans-Meerwein-Straße 4, 35032 Marburg, Germany

[2]Institute of Applied Physics (IAP), Justus Liebig University Gießen, Heinrich-Buff-Ring 16, 35392 Gießen, Germany

[3]Center for Materials Research (LaMa), Justus Liebig University Gießen, Heinrich-Buff-Ring 16, 35392 Gießen, Germany

[4]Institute of Chemistry, Carl von Ossietzky University Oldenburg, Carl-von-Ossietzky-Straße 9-11, 26111 Oldenburg, Germany

[5]Theoretical Chemistry and Interdisciplinary Center for Molecular Materials (ICMM), Department of Chemistry and Pharmacy, Friedrich-Alexander-Universität Erlangen-Nürnberg, Egerlandstraße 3, 91058 Erlangen, Germany

1. Additional Figures

(a) Yields of 5-5, 5-7 and 7-7 coupling types between azulene units, derived from STM images.

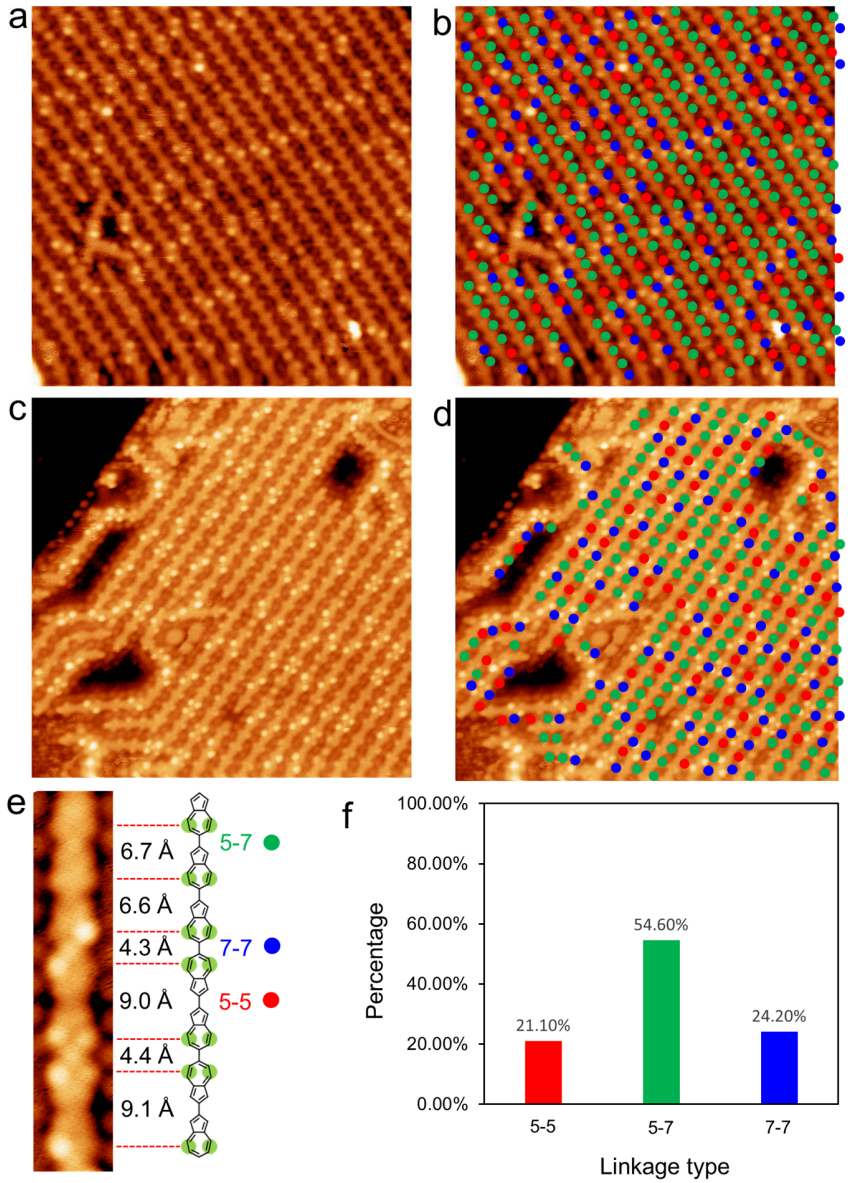

Figure S1. Yield statistics of the 5-5, 5-7 and 7-7 coupling types in polyazulene chains formed on Au(111). (a,c) STM images of two different regions of ordered polyazulene chain domains prepared by the same procedure as in Figure 2a. (b,d) Identical STM images as in panels (a) and (c) overlaid with red, green and blue spheres labeling 5-5, 5-7 and 7-7 coupling types, respectively. (e) Submolecularly resolved STM image of a single polyazulene chain illustrating the discrimination of 5-5, 5-7 and 7-7 coupling types by the distances between the protrusion pairs. The protrusion pair features observed in the STM image correspond to the outer periphery of the seven-membered ring of the azulene unit as marked by the two green dots on the chemical structure. (f) Statistics of the yield (in %) of the 5-5, 5-7, and 7-7 coupling types obtained from the two STM images in panel (a) and (c) by counting a total number of 744 connections.

(b) Figures S2a,b and S2d,e show the STM and nc-AFM images of other phagraphene and TPH-graphene nanoribbons on the same sample as that in Figure 3a of the main text, respectively. Their chemical structures are derived as shown by Figure S2c and Figure S2f, respectively.

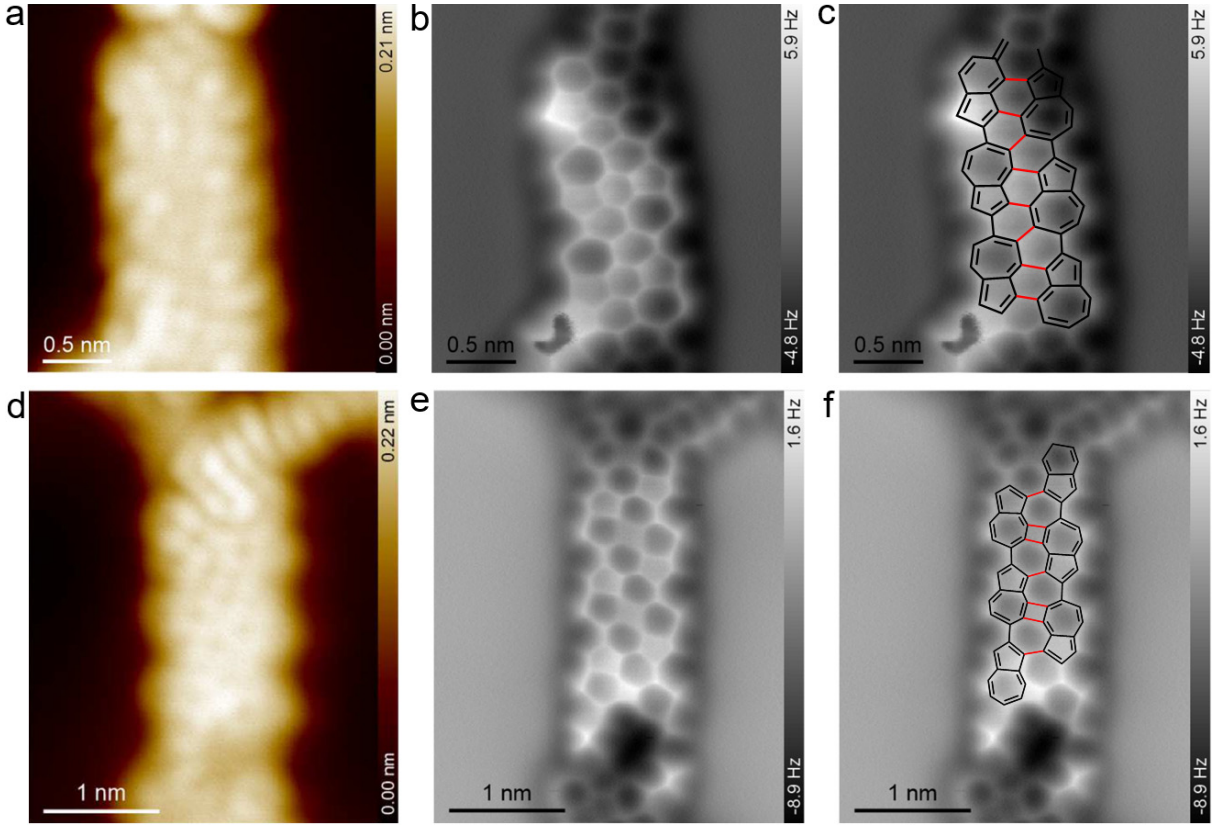

Figure S2. Additional STM and nc-AFM images of phagraphene and TPH-graphene nanoribbons on Au(111). (a-c) High resolution STM (a), nc-AFM (b) images and the overlaid chemical structure (c) of another short phagraphene nanoribbon from the sample in Figure 3a of the main text. (d-f) High resolution STM (d), nc-AFM (e) images and overlaid chemical structure (f) of another short TPH-graphene nanoribbon from the sample in Figure 3a of the main text. Tunneling parameters for the STM images: (a),(d) U = 10 mV, I = 10 pA. Tip distances for the constant-height AFM images: (b) z = 100 pm, and (e) z = 50 pm with respect to the STM set point of I = 10 pA and U = 10 mV above Au(111) substrate.

(c) The two possible resonance structures of the 5-6-5-7-5 fused-ring moiety.

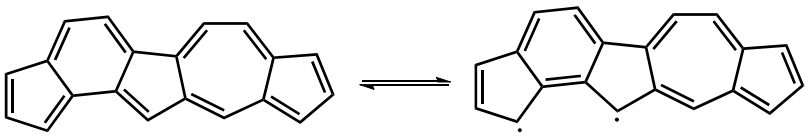

Figure S3. Resonance structures of the fused 5-6-5-7-7 ring moiety.

(d) Annealing of the sample to 780 K leads to extensive rearrangement resulting in the formation of hexagonal rings. As shown by Figures S4a and S4b, the wide carbon nanoribbons are more curved than that in Figures 3a and 3e. This is due mainly to the formation of a high percentage of hexagonal rings as demonstrated by the zoom-in nc-AFM image in Figure S4c. The derived carbon skeleton of this carbon nanoribbon section is displayed in Figure S4d. Only two azulene moieties (red colored) are left in the structure indicating that carbon hexagonal rings are more stable than the five- and seven-membered rings. Occasionally, naphthalene units are also observed in single-row chain as shown by Figures S4e-g.

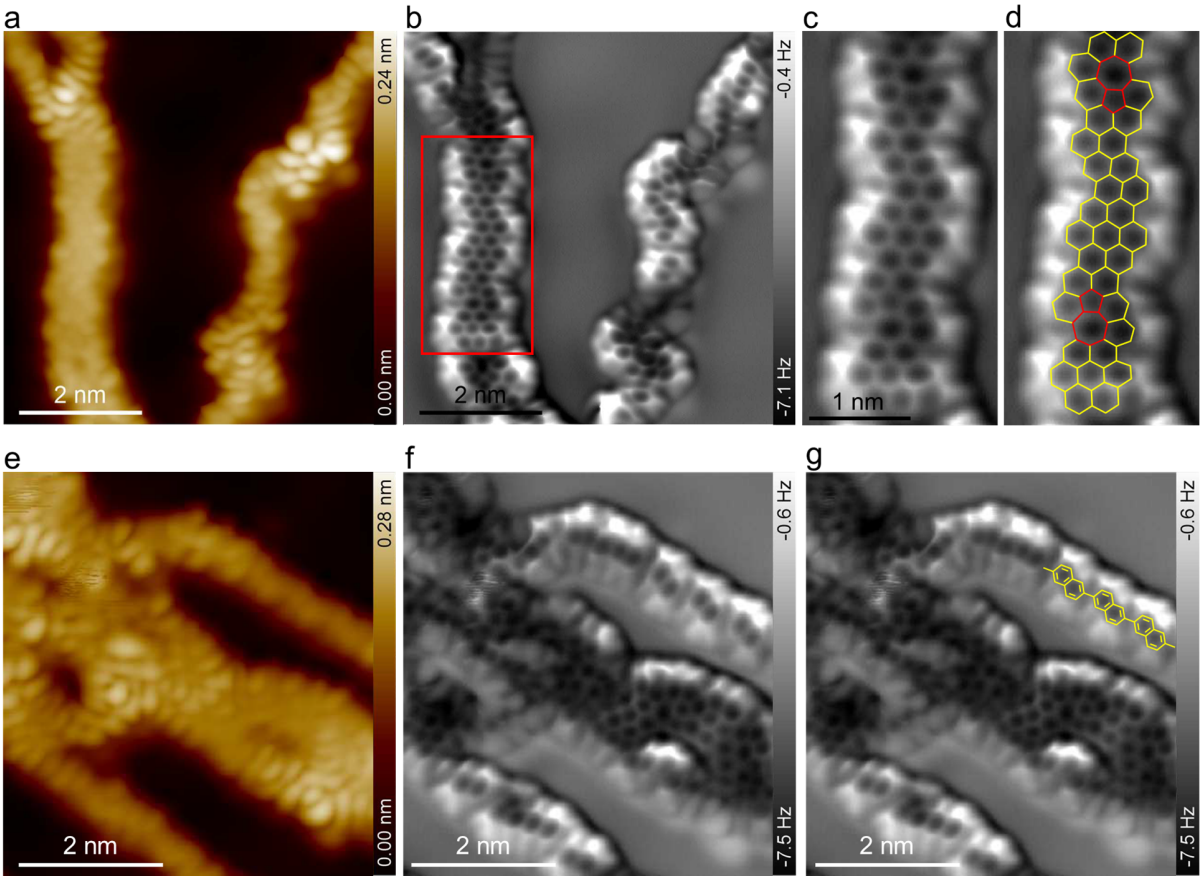

Figure S4. STM and nc-AFM images of the carbon nanoribbons on Au(111) at 780 K. (a,b) Constant-current nc-AFM images showing the topographical (a) and frequency shift (b) channels of carbon nanoribbons obtained by directly annealing the sample to 793 K for 30 minutes. (c,d) Zoom-in constant-current frequency shift image (c) and the derived carbon skeleton (d) of the section of carbon nanoribbon in the red-framed region in panel (b). (e,f) Constant-current nc-AFM images showing the topographical (e) and frequency shift (f) channels of another region on the same sample as in panel (a). (g) The frequency shift image in panel (f) overlaid with molecular structure. The frequency shift images in constant-current mode are measured with topographical STM image feedback at U = 10 mV and I = 100 pA.[1]

(e) DFT-calculated band structures of the phagraphene **6**, TPH-graphene **7** nanoribbons and their alternant counterparts **8** and **9**.

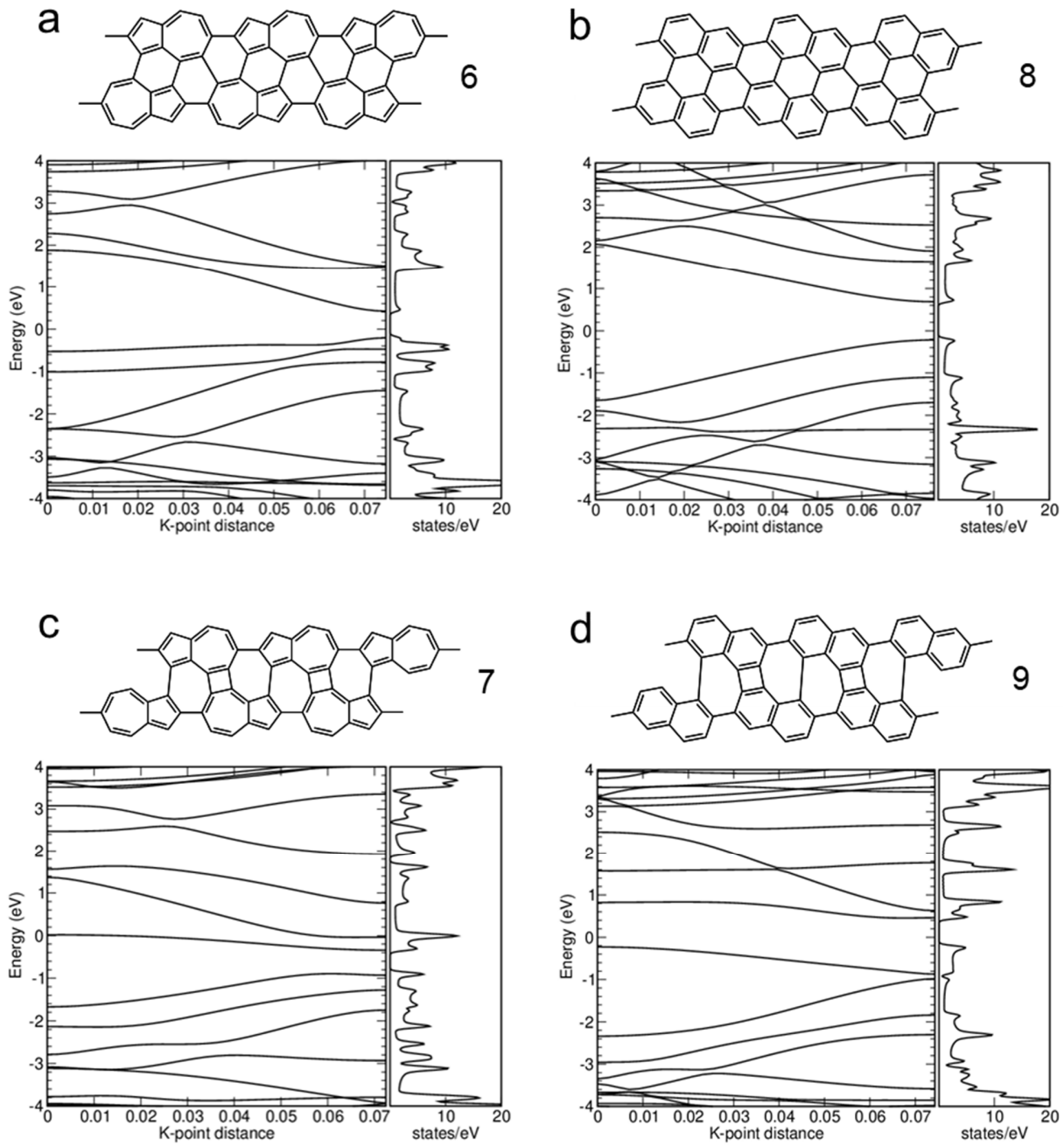

Figure S5. DFT-GGA-calculated band structures of carbon nanoribbons. Molecular and band structures (with density of states) of the nonalternant phagraphene **6** (a), THP graphene **7** (c) nanoribbon and their corresponding alternant graphene nanoribbon counterparts **8** (b) and **9** (d) (PBE functional, 64x1x1 k-points, p4vasp program).

2. Computational Details

Periodic density-functional theory calculations of the planar, free-standing (*i.e.*, without the Au(111) substrate) one-dimensional nanoribbons (cf. Figure 4 of the main paper) were performed with the Vienna Ab Initio Simulation Package (VASP).[2] The PBE functional[3] was used in combination with the third-generation van der Waals dispersion correction due to Grimme (DFT-D3(BJ))[4,5] and the projector-augmented wave (PAW) ansatz[6,7] for the atomic cores. A plane-wave cutoff energy of 520 eV was employed. The orthorhombic unit cells contained a $C_{20}H_6$ formula unit for each system, which was periodically repeated in one dimension. The distance to the periodic images in each of the other two directions (*i.e.*, perpendicular to the direction of propagation of the nanoribbon) was about 10 Å. The cell dimensions as well as the atomic positions were optimized using a force convergence criterion of $5 \cdot 10^{-3}$ eV/Å or better. Note that the atoms were strictly kept in a perfect plane within the orthorhombic cell, *i.e.*, no out-of-plane distortions were possible; the resulting free-standing structures hence do not necessarily represent local minima on the energy hypersurface in the absence of the Au(111) substrate. A 32×1×1 Monkhorst-Pack k-point mesh was used. Geometries are provided in VASP POSCAR format at the end of this file.

3. Synthesis of 2,6-Dibromoazulene

General Information

All reactions with air or water sensitive starting materials were carried out under nitrogen atmosphere in heat-gun-dried glassware using Schlenk techniques. Benzene and ethanol were stored over molecular sieves (3 Å) under nitrogen atmosphere. Column chromatography was carried out on Macherey-Nagel silica gel 60 (230–400 mesh). For thin layer chromatography Merck TLC plates (Silica 60, F254 with fluorescence indicator) were used. ^{1}H and ^{13}C NMR spectra were either recorded on a Bruker Avance 300 (^{1}H NMR: 300 MHz, ^{13}C NMR: 75 MHz) or Avance III (^{1}H NMR: 500 MHz, ^{13}C NMR: 125 MHz). For EI and EI-HRMS a *Finnigan MAT 95* or a *DFS High Resolution Magnetic Sector MS* (*Thermo Scientific*) with an energy of 70 eV and for ESI-HRMS a *Q-TOF Premier* (*Waters*) were used. IR spectra were recorded on a Bruker Tensor 27 (FTIR) spectrometer.

Synthesis scheme

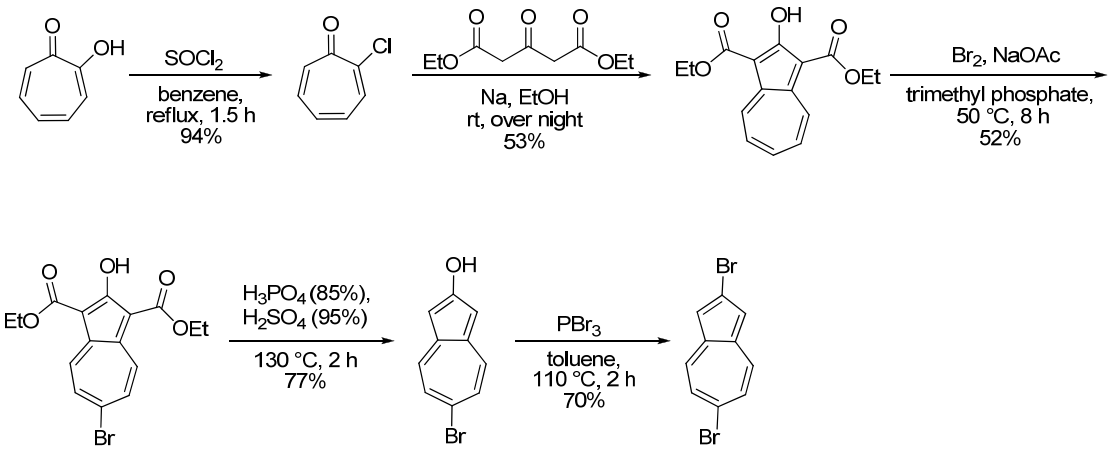

2-Chlorocyclohepta-2,4,6-trien-1-one

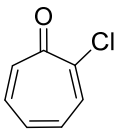

According to a procedure of Marson[8] under nitrogen atmosphere α-tropolone (2.20 g, 18.0 mmol, 1.00 equiv.) was dissolved in anhydrous benzene (55 mL). $SOCl_2$ (1.7 mL, 23.4 mmol, 1.30 equiv.) was added dropwise and the mixture was stirred for 2.5 h at 95 °C. The solvent was removed under vacuum and the crude product was purified by column chromatography (CH_2Cl_2:methanol = 40:1). The product was obtained in 94% yield (2.37 g, 16.9 mmol) as brown solid.

^{1}H NMR (300 MHz, $CDCl_3$, ppm): δ = 7.79 (dd, *J* = 9.3, 0.9 Hz, 1H), 7.25–7.19 (m, 2H), 7.12–7.02 (m, 1H), 6.93 (ddt, *J* = 10.6, 9.4, 1.0 Hz, 1H).

^{13}C NMR (75 MHz, $CDCl_3$, ppm): δ = 180.2, 149.0, 138.6, 135.9, 135.7, 134.2, 131.6.

HRMS (ESI, +): calcd for C_7H_5ONaCl: 162.9927, found 162.9921.

IR (film, cm^{-1}): 3032, 2360, 2159, 2029, 1957, 1626, 1575, 1504, 1457, 1372, 1270, 1243, 1213, 1064, 975, 902, 865, 777, 669, 631.

The analytical data for the ^{1}H NMR spectra is in accordance with the literature.[9]

Diethyl 2-hydroxyazulene-1,3-dicarboxylate

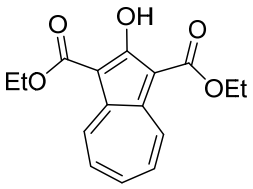

According to a procedure of Marson[8] under nitrogen atmosphere sodium (1.44 g, 62.4 mmol, 26.8 equiv.) was added in portions to anhydrous EtOH (32 mL). Diethyl 3-oxopentanedionate (1.46 g, 4.24 mmol, 3.08 equiv.) was added dropwise and the reaction mixture turned yellow. After adding a solution of 2-chlorocyclohepta-2,4,6-trien-1-one (660 mg, 4.70 mmol, 2.00 equiv.) in anhydrous EtOH (16 mL) the reaction mixture turned dark red and was stirred at ambient temperature overnight. Then, water (50 mL) was added and the reaction mixture was filtered. The solid was dissolved in glacial acetic acid, carefully diluted with water and the aqueous phase was extracted with CH_2Cl_2. The combined organic phase was dried ($MgSO_4$), filtered and concentrated under reduced pressure. The crude product was recrystallized (EtOH) to afford 53% (751 mg, 2.50 mmol) as brown solid.

^{1}H NMR (300 MHz, $CDCl_3$, ppm): δ = 11.75 (s, 1H), 9.30 (s, 2H), 7.66 (s, 3H), 4.49 (q, *J* = 7.2 Hz, 4H), 1.48 (t, *J* = 7.2 Hz, 6H).

^{13}C NMR (75 MHz, $CDCl_3$, ppm): δ = 172.3, 143.4, 136.2, 134.8, 132.5, 101.4, 60.6, 14.7.

The analytical data are in accordance with the literature.[10]

Diethyl 6-bromo-2-hydroxyazulene-1,3-dicarboxylate

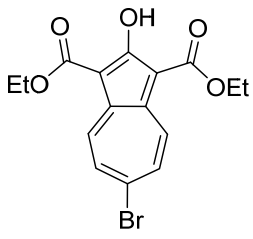

According to a procedure of Tajiri[11] under nitrogen atmosphere diethyl 2-hydroxyazulene-1,3-dicarboxylate (144 mg, 0.50 mmol, 1.00 equiv.) was dissolved in trimethyl phosphate (3.5 mL) and NaOAc (41.0 mg, 0.05 mmol, 1.00 equiv.) was added. Then, bromine (0.05 mL, 1.00 mmol, 2.00 equiv.) was added dropwise and the reaction mixture was stirred 8 h at 50 °C. The mixture was quenched with saturated NH_4Cl solution (10%) and the phases were separated. The aqueous phase was extracted with CH_2Cl_2 and the combined organic phase was dried ($MgSO_4$) and filtered. The solvent was removed under reduced pressure and the crude product was purified by column chromatography (CH_2Cl_2:MeOH = 40:1). The product was obtained in 52% yield (96 mg, 0.26 mmol) as pale yellow solid.

^{1}H NMR (300 MHz, $CDCl_3$, ppm): δ = 11.68 (s, 1H), 8.94 (d, *J* = 11.3 Hz, 2H), 7.93–7.85 (m, 2H), 4.48 (q, *J* = 7.1 Hz, 4H), 1.47 (t, *J* = 7.1 Hz, 6H).

^{13}C NMR (75 MHz, $CDCl_3$, ppm): δ = 172.3, 166.4, 141.5, 135.3, 132.8, 132.7, 102.7, 60.8, 14.6. $C_{q,Br}$ is not detectable.

HRMS (ESI, +): calcd for $C_{16}H_{14}O_5Br$: 365.0025, found 365.0023.

IR (film, cm^{-1}): 2922, 2354, 2196, 1957, 1660, 1583, 1523, 1471, 1439, 1382, 1331, 1252, 1166, 1021, 999, 929, 859, 831, 790, 693, 680, 627.

The analytical data for the ^{1}H NMR spectra are in accordance with the literature.[11]

6-Bromoazulen-2-ol

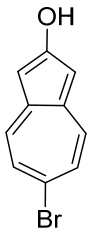

According to a procedure of Lörtscher[12] diethyl 6-bromo-2-hydroxyazulene-1,3-dicarboxylate (150 mg, 0.40 mmol, 1.00 equiv.) was dissolved in 95% H_2SO_4 (15 mL). Carefully 85% H_3PO_4 (75 mL) was added and the reaction mixture was stirred 2 h at 130 °C. After cooling down to ambient temperature the reaction mixture was poured into ice water. The aqueous phase was extracted with Et_2O, dried ($MgSO_4$) and filtered. After removal of solvent the crude product was purified by column chromatography (CH_2Cl_2:Et_2O = 9:1). The product was obtained in 77% yield (70.0 mg, 0.30 mmol) as dark red solid.

^{1}H NMR (300 MHz, DMSO-d_6, ppm): δ = 11.22 (s, 1H), 7.81 (d, *J* = 10.9 Hz, 2H), 7.48 (d, *J* = 10.9 Hz, 2H), 6.81 (s, 2H).

^{13}C NMR (75 MHz, DMSO-d_6, ppm): δ = 168.7, 138.7, 128.7, 126.8, 126.2, 105.5.

The analytical data are in accordance with the literature.[12]

2,6-Dibromoazulene

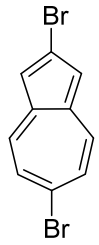

According to a procedure of Lörtscher[12] 6-bromoazulen-2-ol (100 mg, 0.45 mmol, 1.00 equiv.) was dissolved in toluene (60 mL). Then PBr_3 (0.13 mL, 1.36 mmol, 3.00 equiv.) was added dropwise and the reaction mixture was stirred 2 h at 110 °C. After cooling down to ambient temperature the reaction mixture was poured into ice water. The phases were separated and the aqueous phase was extracted with toluene. The combined organic phase was washed with water, dried ($MgSO_4$) and filtered. The solvent was removed under reduced pressure and the crude product was purified by column chromatography (*n*-pentane:CH_2Cl_2 = 9:1). The product was obtained in 70% yield (90.0 mg, 0.31 mmol) as purple solid.

^{1}H NMR (300 MHz, DMSO-d_6, ppm): δ = 8.20 (d, *J* = 10.4 Hz, 2H), 7.70 (d, *J* = 10.1 Hz, 2H), 7.54 (s, 2H).

^{13}C NMR (75 MHz, DMSO-d_6, ppm): δ = 139.0, 135.0, 133.8, 128.6, 128.6, 121.2.

MS (EI) *m/z* (%): 286 (33, [M^+]), 284 (17), 208 (1), 205 (9), 204 (1), 143 (3), 127 (9), 126 (100), 125(7), 104 (1), 100 (5), 99 (9), 87 (6), 76 (9), 74 (15), 63 (28), 62 (9), 50 (11).

HRMS (EI, *m*/*z*): calcd for $C_{10}H_6Br_2$: 283.8831, found 283.8827.

IR (film, cm^{-1}): 2928, 2209, 2148, 1917, 1573, 1521, 1466, 1435, 1389, 1283, 1215, 1072, 1011, 971, 853, 832, 815, 786, 723, 701, 608.

The analytical data are in accordance with the literature.[12]

NMR Spectra

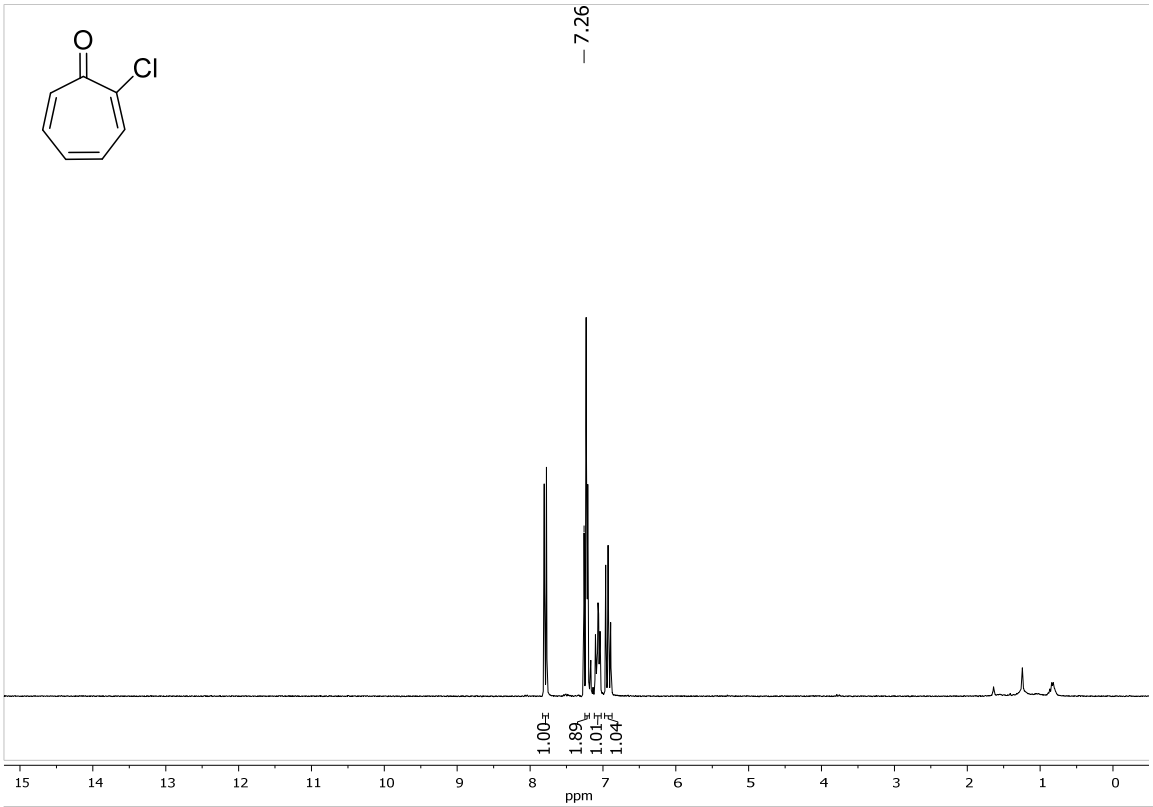
O
Cl
7.26
1.00
1.89
1.01
1.04
15 14 13 12 11 10 9 8 7 6 5 4 3 2 1 0
ppm

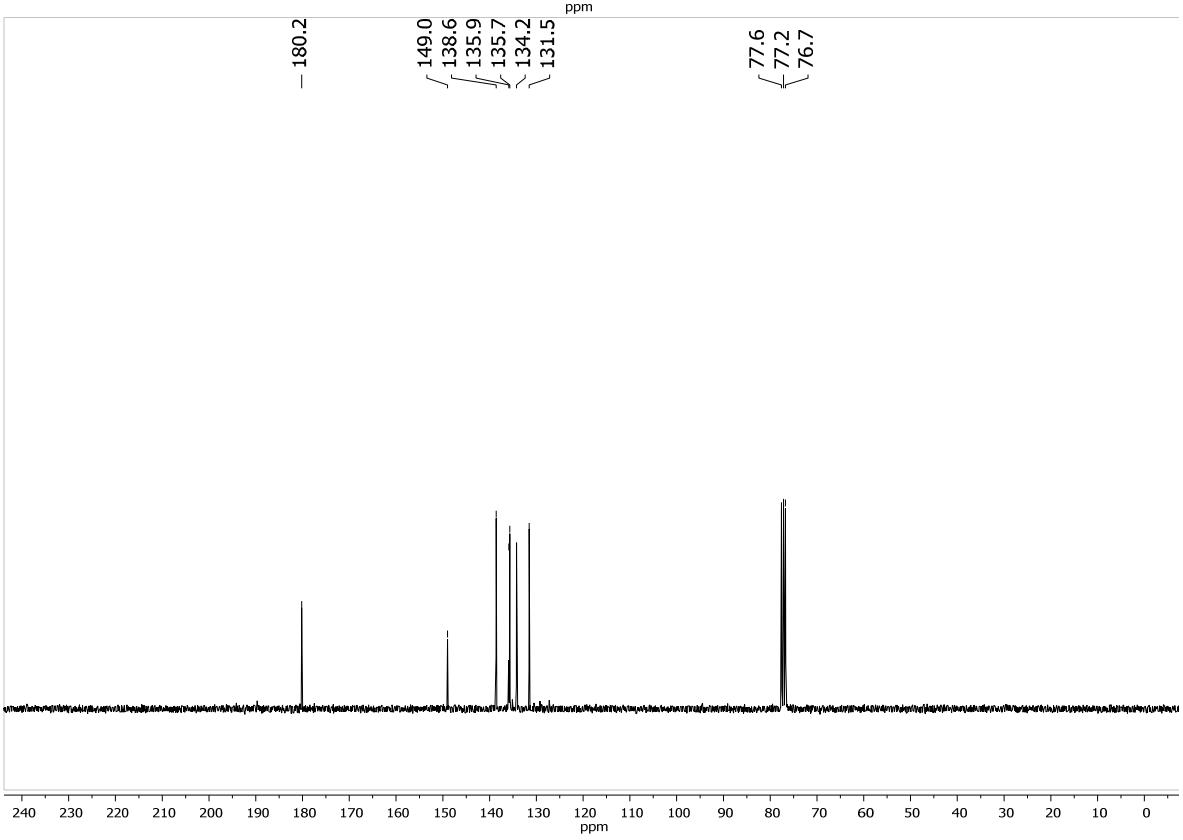
180.2
149.0
138.6
135.9
135.7
134.2
131.5
77.6
77.2
76.7
240 230 220 210 200 190 180 170 160 150 140 130 120 110 100 90 80 70 60 50 40 30 20 10 0
ppm

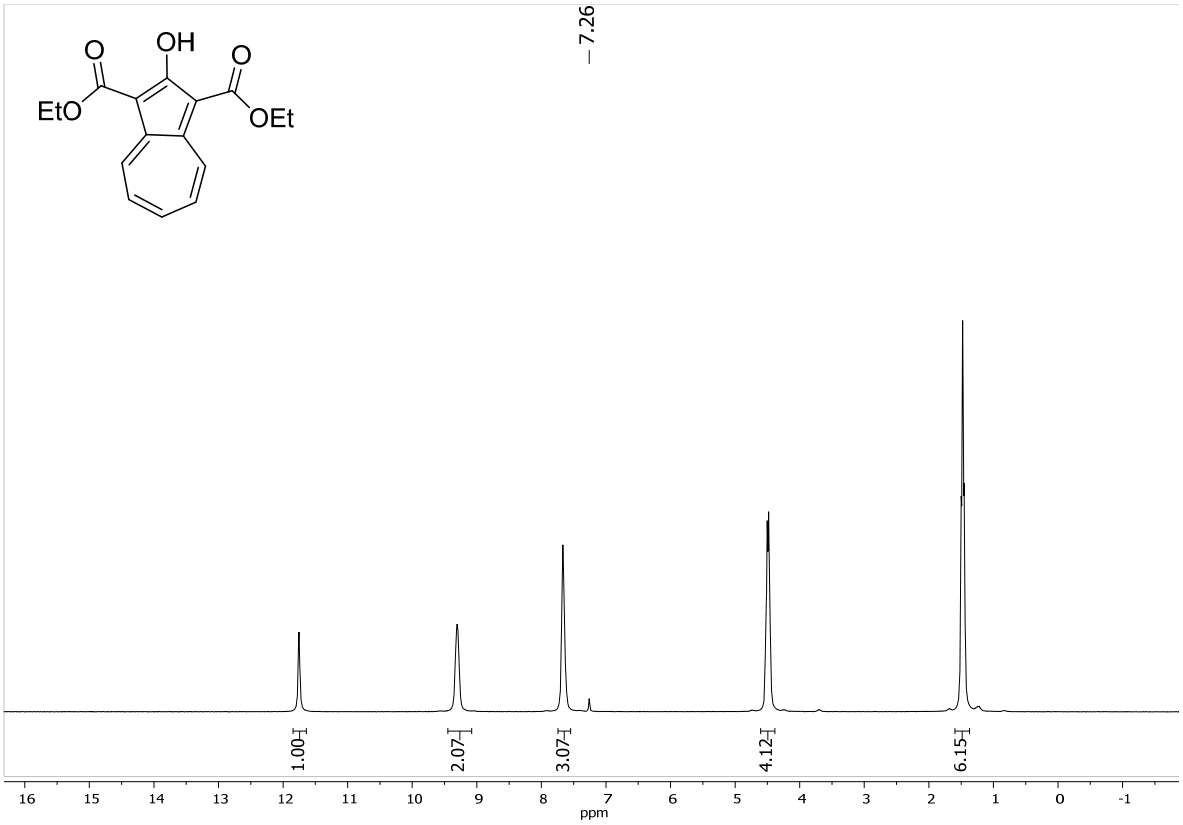
O
OH
O
EtO
OEt
7.26
1.00
2.07
3.07
4.12
6.15
ppm

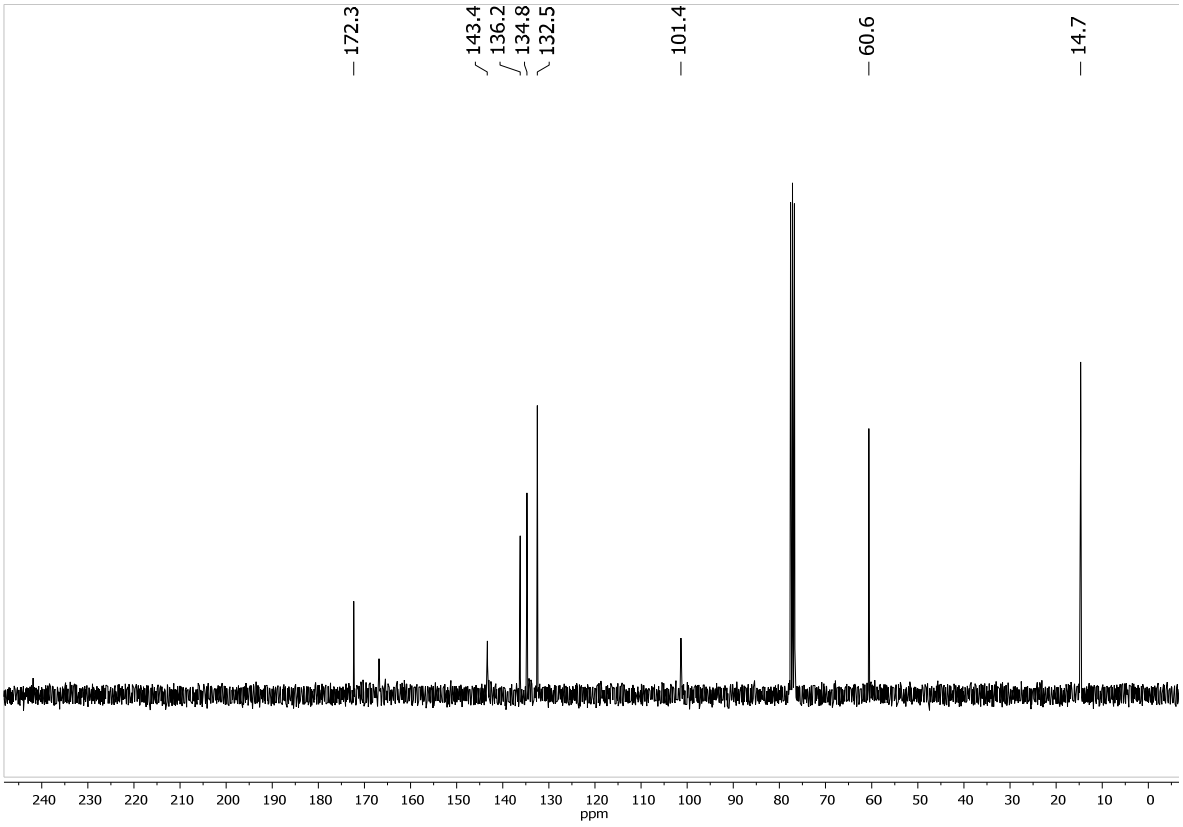
172.3
143.4
136.2
134.8
132.5
101.4
60.6
14.7
ppm

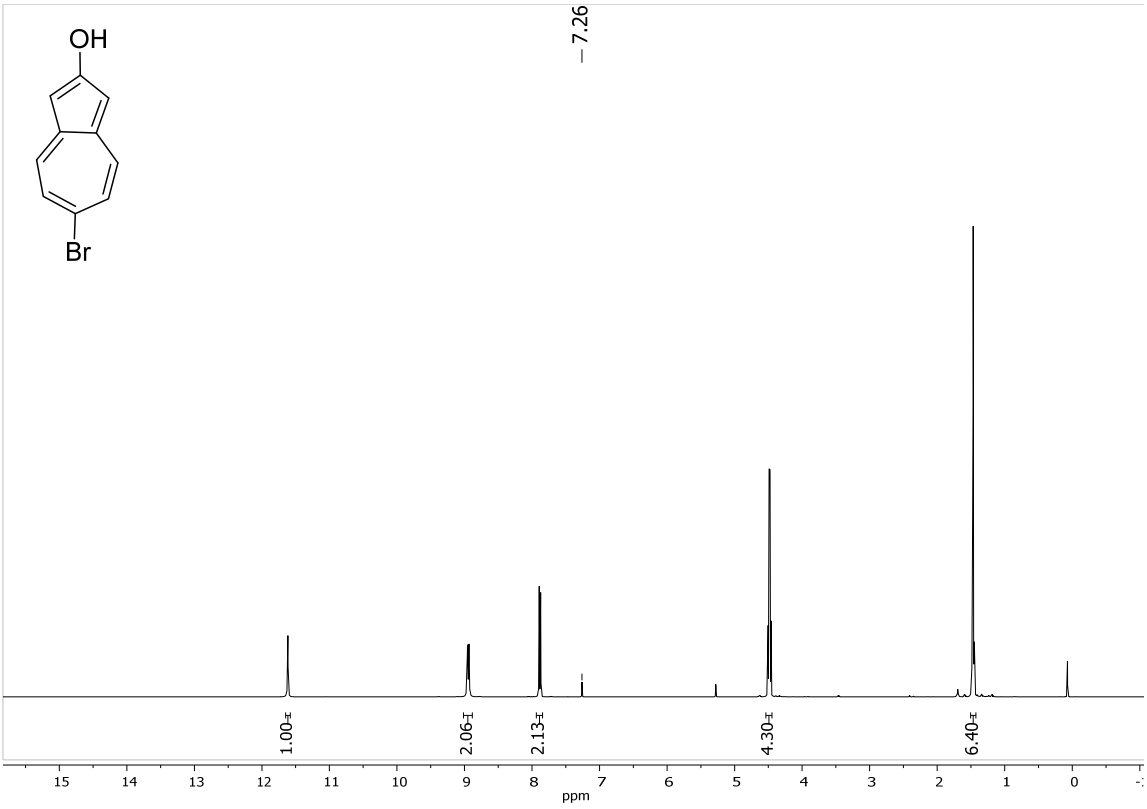
OH
Br
7.26
1.00
2.06
2.13
4.30
6.40
ppm

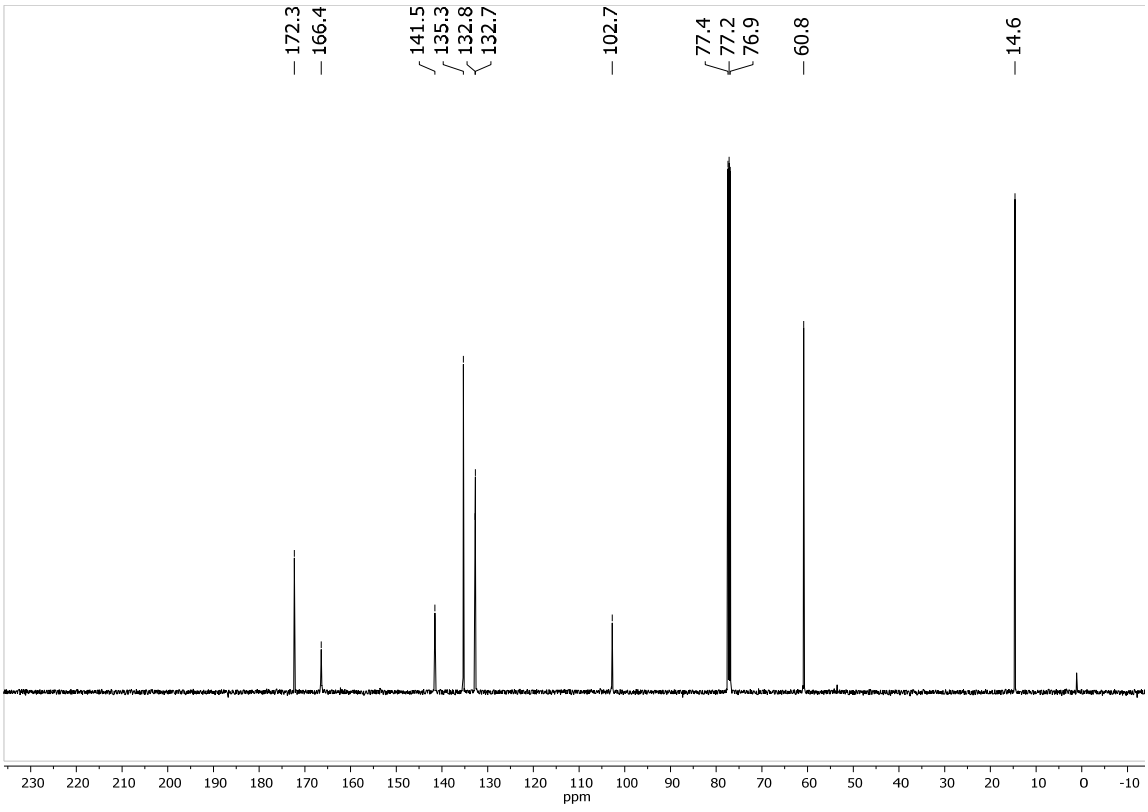
172.3
166.4
141.5
135.3
132.8
132.7
102.7
77.4
77.2
76.9
60.8
14.6
ppm

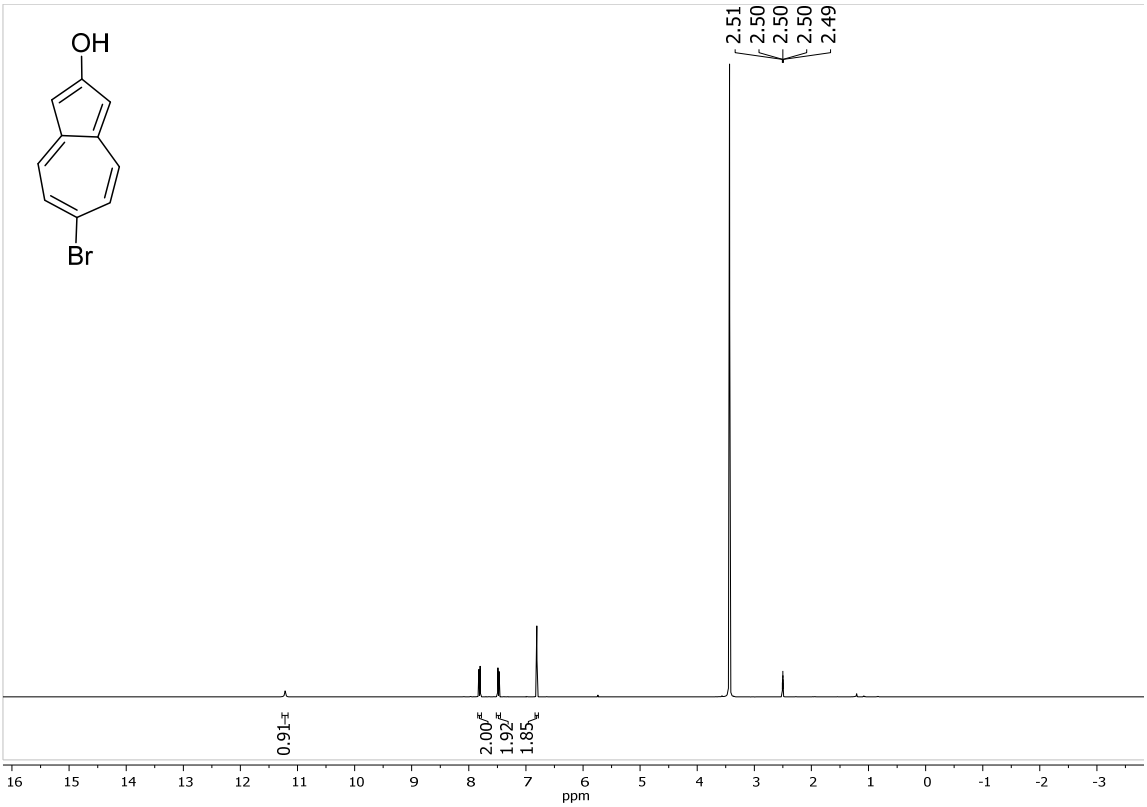
OH
Br
2.51
2.50
2.50
2.50
2.49
0.91
2.00
1.92
1.85
16 15 14 13 12 11 10 9 8 7 6 5 4 3 2 1 0 -1 -2 -3
ppm

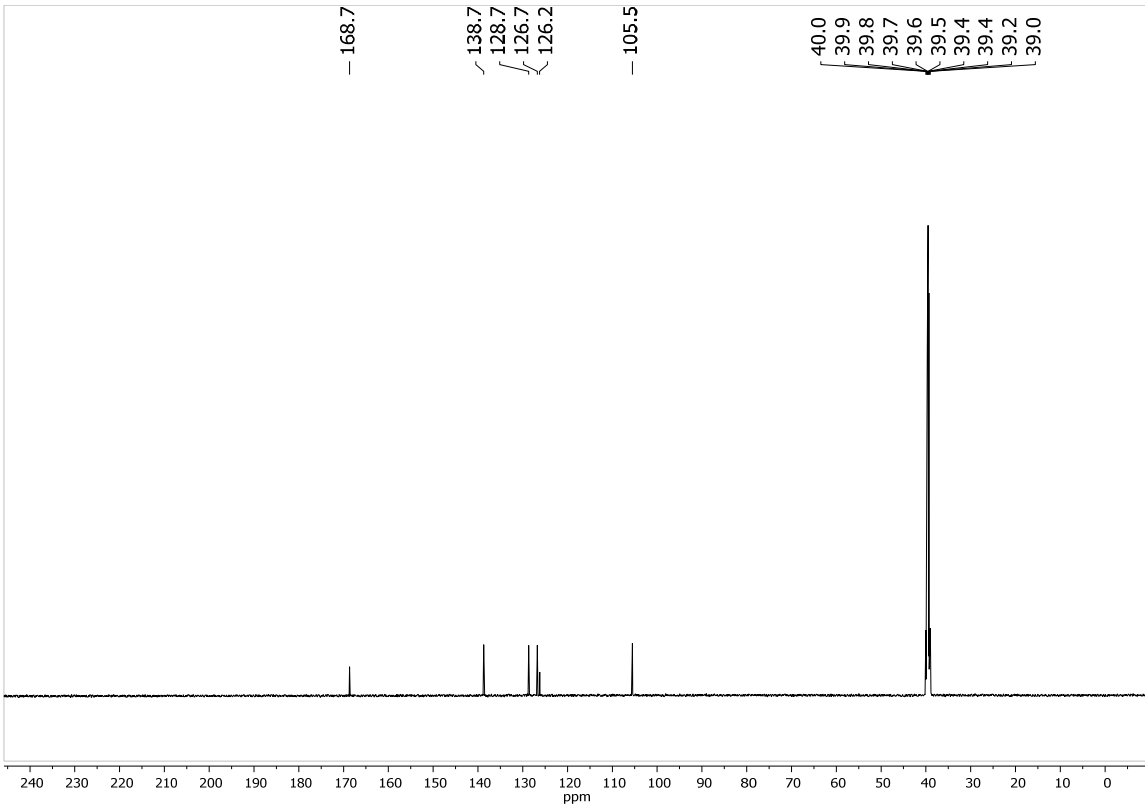
168.7
138.7
128.7
126.7
126.2
105.5
40.0
39.9
39.8
39.7
39.6
39.5
39.4
39.4
39.2
39.0
240 230 220 210 200 190 180 170 160 150 140 130 120 110 100 90 80 70 60 50 40 30 20 10 0
ppm

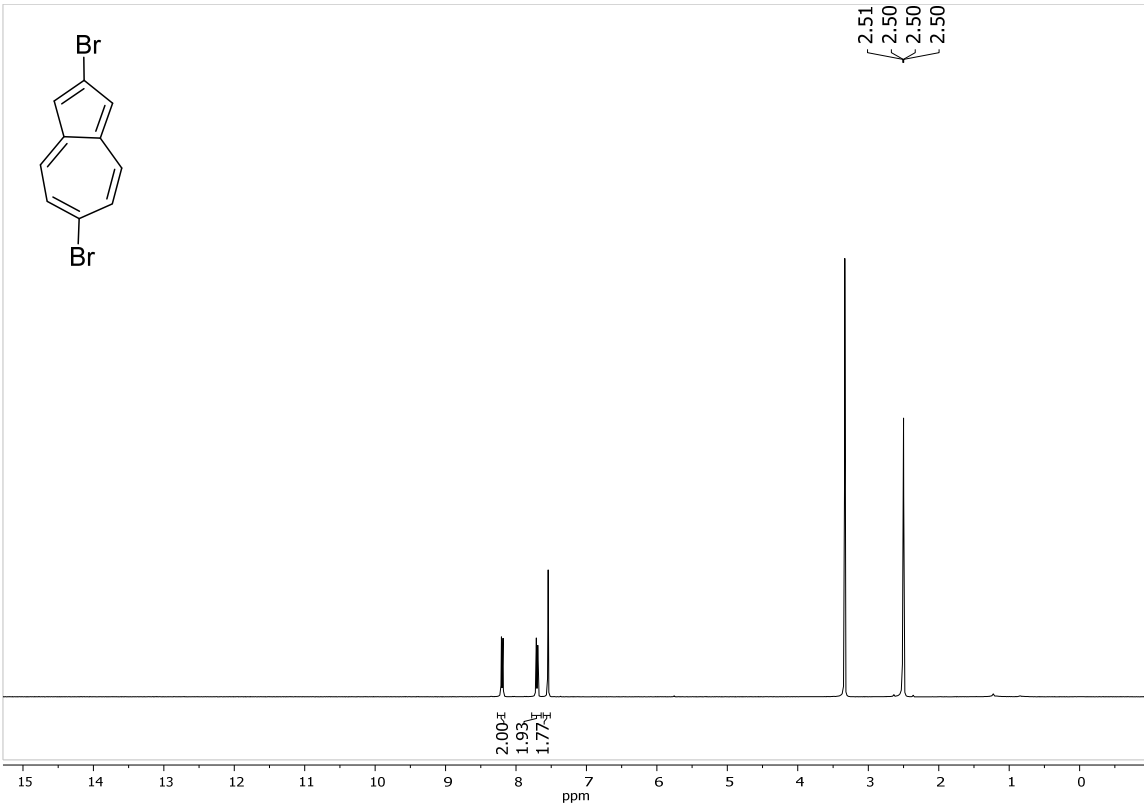
Br
Br
2.51
2.50
2.50
2.50
2.00
1.93
1.77
15
14
13
12
11
10
9
8
7
6
5
4
3
2
1
0
ppm

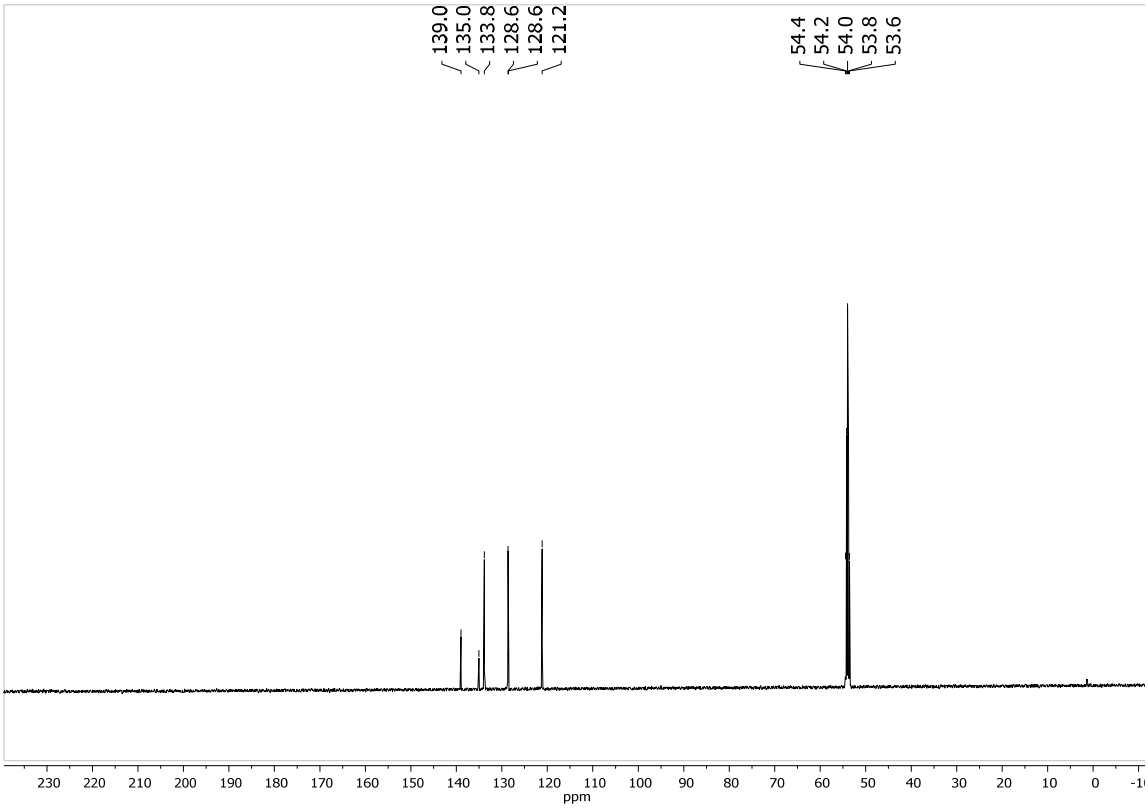
139.0
135.0
133.8
128.6
128.6
121.2
54.4
54.2
54.0
53.8
53.6
230
220
210
200
190
180
170
160
150
140
130
120
110
100
90
80
70
60
50
40
30
20
10
0
ppm

4. DFT-Optimized Geometries (VASP POSCAR format):

Phagraphene **6**, cf. Figure 4a

```
  1.00000000000000
    6.6933222301648030    0.0000000000000000    0.0000000000000000
    0.0000000000000000   19.9945370318452902    0.0000000000000000
    0.0000000000000000    0.0000000000000000    9.9972685159226451
  C    H
   20    6
Direct
  0.9305023410464344  0.3394975141631420  0.5000000000000000
  0.0290385604536638  0.4031389438167139  0.5000000000000000
  0.9456387273584070  0.4702014666864542  0.5000000000000000
  0.7351179547437212  0.3188885303525808  0.5000000000000000
  0.7803135639196412  0.6033104957089392  0.5000000000000000
  0.7285108422307900  0.4800266830727509  0.5000000000000000
  0.6543585396131277  0.5460251343961318  0.5000000000000000
  0.6555661236073220  0.6605905892804387  0.5000000000000000
  0.5663321908942223  0.3601968541395237  0.5000000000000000
  0.5711595917440775  0.4327139251851833  0.5000000000000000
  0.4506922372100277  0.5667533743363649  0.5000000000000000
  0.4555288328989349  0.6392688257777976  0.5000000000000000
  0.3662827196248344  0.3388920803383328  0.5000000000000000
  0.3674883650829770  0.4534474021106618  0.5000000000000000
  0.2933226376518192  0.5194430165521453  0.5000000000000000
  0.2415149782669914  0.3961740352515761  0.5000000000000000
  0.2867073612571289  0.6805651728391595  0.5000000000000000
  0.0761856021821927  0.5292722275961950  0.5000000000000000
  0.0912908199085720  0.6599714333525029  0.5000000000000000
  0.9928061539280719  0.5963320207166944  0.5000000000000000
  0.0361576307303793  0.2981237171173845  0.5000000000000000
  0.9856650579254662  0.7013576983531635  0.5000000000000000
  0.7090710385150913  0.2649022718186416  0.5000000000000000
  0.6993319232195176  0.7129130763694604  0.5000000000000000
  0.3224626099758936  0.2865767022266468  0.5000000000000000
  0.3127314594225936  0.7345570152564846  0.5000000000000000
```

Naphthalene analogue of phagraphene **8**, cf. Figure 4b

```
  1.00000000000000
    6.5528376349350159    0.0000000000000000    0.0000000000000000
    0.0000000000000000   19.5748763094411302    0.0000000000000000
    0.0000000000000000    0.0000000000000000    9.7874381546716300
  C    H
   20    6
Direct
  0.8653258480143720  0.3492306889336945  0.5000000000050022
  0.0094001328428419  0.4018121695727856  0.5000000000050022
  0.9379851982139016  0.4712251848127238  0.5000000000050022
```

0.6548350100065221 0.3618272947835450 0.5000000000050022
0.7914764955701372 0.6095119748314985 0.5000000000050022
0.7245780322489139 0.4850542230804891 0.5000000000050022
0.6521716144290437 0.5543453669559639 0.5000000000050022
0.7130562993056060 0.6774008751433485 0.5000000000050022
0.5107689254690726 0.3074410383642956 0.5000000000050022
0.5814366686987142 0.4306170157789211 0.5000000000050022
0.4369921213446091 0.5670574275602149 0.5000000000050022
0.5076626711675232 0.6902119722268054 0.5000000000050022
0.3053483058644986 0.3202527729239222 0.5000000000050022
0.3663056051860494 0.4433245139469477 0.5000000000050022
0.2938543541446634 0.5126085816878998 0.5000000000050022
0.2269389071126540 0.3881655107484292 0.5000000000050022
0.3635895656498889 0.6358327493337299 0.5000000000050022
0.0804341532854949 0.5264479760825083 0.5000000000050022
0.1530944470044062 0.6484408763329341 0.5000000000050022
0.0090259306777440 0.5958807664944743 0.5000000000050022
0.9139417094045257 0.2960202405113677 0.5000000000050022
0.1044575666305576 0.7016456882573010 0.5000000000050022
0.5671465671890417 0.2549604210370688 0.5000000000050022
0.8178592296189180 0.7205279770812325 0.5000000000050022
0.2005335542879223 0.2771225269064956 0.5000000000050022
0.4512174879421593 0.7426806795184930 0.5000000000050022

TPH-graphene **7**, cf. Figure 4c
1.00000000000000
6.9002423548684684 0.0000000000000000 0.0000000000000000
0.0000000000000000 20.2189499257740728 0.0000000000000000
0.0000000000000000 0.0000000000000000 10.1094749628870364
C H
20 6
Direct
0.0815348043163553 0.5357428678466292 0.5000000000000000
0.0812551038581120 0.6521626007503940 0.5000000000000000
0.2052645485360571 0.5954048356667627 0.5000000000000000
0.8890435965752346 0.5622063650214173 0.5000000000000000
0.8859744874933781 0.6338727711893171 0.5000000000000000
0.7828407082244908 0.3988456907530491 0.5000000000000000
0.6784469975878551 0.3367440191434170 0.5000000000000000
0.7235724052107173 0.5261467923466228 0.5000000000000000
0.7182647490882772 0.6757182047884811 0.5000000000000000
0.6769982158039909 0.4565504186474740 0.5000000000000000
0.4800879416911101 0.3243766453062733 0.5000000000000000
0.5211388607940322 0.5435722799038558 0.5000000000000000
0.5198855621450917 0.6633737938843751 0.5000000000000000
0.4745588698611201 0.4739692575093528 0.5000000000000000
0.4153819916186734 0.6012967452841167 0.5000000000000000
0.3122899657209572 0.3662238455282605 0.5000000000000000

0.3091299497072484 0.4379048229710136 0.5000000000000000
0.1169648306246742 0.3479596964627518 0.5000000000000000
0.1166743771283336 0.4643901847573488 0.5000000000000000
0.9929480698412334 0.4047396342213219 0.5000000000000000
0.1329869986440997 0.7029749828361957 0.5000000000000000
0.7674892941215177 0.2921784018458808 0.5000000000000000
0.7547277330022482 0.7284194544792157 0.5000000000000000
0.4436625591963974 0.2716718774199265 0.5000000000000000
0.4309041287440039 0.7079529558257818 0.5000000000000000
0.0652197660563374 0.2971475846256482 0.5000000000000000

Naphthalene analogue of TPH-graphene **9**, cf. Figure 4d
1.00000000000000
6.7287360850331259 0.0000000000000000 0.0000000000000000
0.0000000000000000 19.7164057390543164 0.0000000000000000
0.0000000000000000 0.0000000000000000 9.8582028695758837
C H
20 6
Direct
0.0829007128662931 0.5450467719134585 0.5000000000000000
0.1402261862356685 0.6715111026105045 0.5000000000000000
0.2178411374127576 0.6033316109000877 0.5000000000000000
0.8797140138362507 0.5699085636642205 0.5000000000000000
0.9453774310170878 0.6910643943978845 0.5000000000000000
0.7540202183910338 0.3945621529443262 0.5000000000000000
0.6014618444719868 0.3437431171797558 0.5000000000000000
0.7238275792198747 0.5267021540632593 0.5000000000000000
0.7988059615934551 0.6399713963658200 0.5000000000000000
0.6679565588877067 0.4561249391842058 0.5000000000000000
0.3933958336708990 0.3599858770747774 0.5000000000000000
0.5243226899776794 0.5438183644564124 0.5000000000000000
0.5907636580511260 0.6562105405810650 0.5000000000000000
0.4684696626523568 0.4732453709747688 0.5000000000000000
0.4382219299771296 0.6053855337490107 0.5000000000000000
0.2468775411450346 0.3088793919018351 0.5000000000000000
0.3125716228959664 0.4300474242726509 0.5000000000000000
0.0520292056255809 0.3284317986983409 0.5000000000000000
0.1093526585314196 0.4548937164121816 0.5000000000000000
0.9743985438061279 0.3966114797991578 0.5000000000000000
0.2525485012942588 0.7113052536379276 0.5000000000000000
0.6357243590975168 0.2896145389556261 0.5000000000000000
0.9048986387146201 0.7446689191078132 0.5000000000000000
0.2874086917371503 0.2552835510013876 0.5000000000000000
0.5565038567264934 0.7103425576711522 0.5000000000000000
0.9396879064718606 0.2886472246150026 0.5000000000000000

References

1. Martin-Jimenez, D.; Ahles, S.; Mollenhauer, D.; Wegner, H. A.; Schirmeisen, A.; Ebeling, D. Bond-Level Imaging of the 3D Conformation of Adsorbed Organic Molecules Using Atomic Force Microscopy with Simultaneous Tunneling Feedback. *Phys. Rev. Lett.* **2019,** *122,* 196101.

2. Kresse, G.; Hafner, J. Vienna *Ab Initio* Simulation Package (VASP), version 5.2. *Institut für Materialphysik, Universität Wien, Vienna, since* **1991,** *www.vasp.at*.

3. Perdew, J. P.; Burke, K.; Ernzerhof, M. Generalized Gradient Approximation Made Simple. *Phys. Rev. Lett.* **1996,** *77,* 3865-3868.

4. Grimme, S.; Antony, J.; Ehrlich, S.; Krieg, H. A Consistent and Accurate *ab initio* Parametrization of Density Functional Dispersion Correction (DFT-D) for the 94 Elements H-Pu. *J. Chem. Phys.* **2010,** *132,* 154104.

5. Grimme, S.; Ehrlich, S.; Goerigk, L. Effect of the Damping Function in Dispersion Corrected Density Functional Theory. *J. Comput. Chem.* **2011,** *32,* 1456-1465.

6. Blochl, P. E. Projector Augmented-Wave Method. *Phys. Rev. B* **1994,** *50,* 17953-17979.

7. Kresse, G.; Joubert, D. From Ultrasoft Pseudopotentials to the Projector Augmented-Wave Method. *Phys. Rev. B* **1999,** *59,* 1758-1775.

8. Brettle, R.; Dunmur, D. A.; Estdale, S.; Marson, C. M. Synthesis, Linear Dichroism and Mesogenic Properties of Substituted Azulenes. *J. Mater. Chem.* **1993,** *3,* 327-331.

9. Zhang, J.; Petoud, S. Azulene-Moiety-Based Ligand for the Efficient Sensitization of Four Near-Infrared Luminescent Lanthanide Cations: Nd3+, Er3+, Tm3+, and Yb3+. *Chem. Eur. J.* **2008,** *14,* 1264-1272.

10. Chen, A.-H. Electrochemical Methoxylation of 1,2,3-Trisubstituted Azulenes. *J. Chin. Chem. Soc.* **1999,** *46,* 35-39.

11. Ito, S.; Ando, M.; Nomura, A.; Morita, N.; Kabuto, C.; Mukai, H.; Ohta, K.; Kawakami, J.; Yoshizawa, A.; Tajiri, A. Synthesis and Properties of Hexakis(6-octyl-2-azulenyl)benzene as a Multielectron Redox System with Liquid Crystalline Behavior. *J. Org. Chem.* **2005,** *70,* 3939-3949.

12. Schwarz, F.; Koch, M.; Kastlunger, G.; Berke, H.; Stadler, R.; Venkatesan, K.; Lörtscher, E. Charge Transport and Conductance Switching of Redox-Active Azulene Derivatives. *Angew. Chem. Int. Ed.* **2016,** *55,* 11781-11786.